

# Modeling of the elongation and retraction of *Escherichia coli* P pili under strain by Monte Carlo simulations

Oscar Björnham · Ove Axner · Magnus Andersson

Received: 28 March 2007 / Revised: 17 August 2007 / Accepted: 14 September 2007 / Published online: 10 October 2007  
© EBSA 2007

**Abstract** P pili are fimbrial adhesion organelles expressed by uropathogenic *Escherichia coli* in the upper urinary tract. They constitute a stiff helix-like polymer consisting of a number of subunits joined by head-to-tail bonds. The elongation and retraction properties of individual P pili exposed to strain have been modeled by Monte Carlo (MC) simulations. The simulation model is based upon a three-state energy landscape that deforms under an applied force. Bond opening and closure are modeled by Bells theory while the elongation of the linearized part of the pilus is described by a worm-like chain model. The simulations are compared with measurements made by force measuring optical tweezers. It was found that the simulations can reproduce pili elongation as well as retraction, under both equilibrium and dynamic conditions, including entropic effects. It is shown that the simulations allow for an assessment of various model parameters, e.g. the unfolding force, energy barrier heights, and various distances in the energy landscape, including their stochastic spread that analytical models are unable to do. The results demonstrate that MC simulations are useful to model elongation and retraction properties of P pili, and therefore presumably also other types of pili, exposed to strain and/or stress. MC simulations are particularly suited for description of helix-like pili since these have an intricate self-regulating mechanical elongation behavior that makes analytical

descriptions non-trivial when dynamic processes are studied, or if additional interactions in the rod or the behavior of the adhesion tip needs to be modeled.

**Keywords** P pili · *Escherichia coli* · Optical tweezers · Monte Carlo simulations · Unfolding · Force spectroscopy

## Abbreviations

MC	Monte Carlo
WLC	Worm-like chain
AFM	Atomic Force Microscopy
DFS	Dynamic Force Spectroscopy
UPEC	Uropathogenic <i>E. coli</i>
MCMC	Markov Chain Monte Carlo

## Introduction

The heavy use of antibiotics during the last decades has lead to a high degree of resistance among bacteria. New and refined means to combat bacteria and bacterial infections are therefore urgently needed. Bacteria invading the urinary tract, so called uropathogenic *Escherichia coli* (UPEC), are of particular interest, since they are frequently exposed to shear forces from the urine flow that efficiently remove all bacteria that cannot withstand such forces. They bind to host tissue by fimbrial adhesion organelles, so called pili (Johnson and Russo 2002; Soto and Hultgren 1999). Access to pili with a large degree of flexibility seems to be a necessary prerequisite to sustain shear forces and thereby to survive the cleaning action from urine flow (Bullitt and Makowski 1995; Thomas et al. 2002). One means to find an alternative to antibiotics to cure diseases

O. Björnham  
Department of Applied Physics and Electronics,  
Umeå University, 901 87 Umeå, Sweden

O. Axner · M. Andersson (✉)  
Department of Physics, Umeå University, 901 87 Umeå, Sweden  
e-mail: magnus.andersson@physics.umu.se  
URL: <http://www.phys.umu.se/exphys/OpticalTweezers/index.htm>

caused by UPEC bacteria could thereby be to compromise the flexibility of the pili, for example, by the use of a drug that can target the flexibility of pili. However, in order to find such drugs, new targets in bacterial pili have to be found. It is, therefore, of importance to assess the intrinsic biomechanical properties of the elongation and retraction of pili under strain/stress, both by experiments and by modeling/simulations.

The pili that predominantly are expressed by bacteria in the upper urinary tract are termed P pili (Bullitt and Makowski 1998). A P pilus has, as its main part, a three-dimensional structure, often referred to as the “rod”, which is composed of  $\sim 10^3$  PapA subunits in a helical arrangement (Bullitt and Makowski 1995; Gong and Makowski 1992). As has been shown previously, this construction provides the pili with a large degree of flexibility; it allows for an unfolding of the quaternary structure when a pilus is exposed to strain or stress (Andersson et al. 2006a, b, c; Fällman et al. 2005; Jass et al. 2004). This unfolding reduces the loading rate of the adhesin-receptor bond (Miller et al. 2006) and allows for cooperative bacterial-to-host-cell bindings (Bullitt and Makowski 1995) that distribute an external force among several pili, both of which are believed to increase the bond lifetime and the resistance to shear forces.

The unique role of these pili justifies a detailed assessment of their biomechanical properties. Both measurements and modeling are essential in order to gain knowledge about and understand the intrinsic and molecular behavior of adhesion organelles under *in vivo* conditions. The mechanical behavior of P pili under strain or stress has been explored both by force measuring optical tweezers (FMOT; Andersson et al. 2006a, b, c; Fällman et al. 2004, 2005; Jass et al. 2004) and atomic force microscopy (AFM; Miller et al. 2006). Such measurements have shown, among other things, that P pili exposed to strain or stress can elongate in three distinct regions. As is illustrated in Fig. 1, the first elongation region (for elongations of up to a fraction of its relaxed length, referred to as region I) is characterized by a linear force–elongation response that is considered to originate from an elastic stretching of the quaternary structure of the PapA rod. The second region, referred to as region II, is characterized by an elongation (up to  $\sim 7$  times) under constant force (27 pN under so called steady-state conditions)<sup>1</sup> and has been attributed to an unfolding of the quaternary structure of the PapA rod by a consecutive opening of the outermost layer-to-layer bond (Andersson et al. 2006a, c; Fällman et al. 2005). Finally,

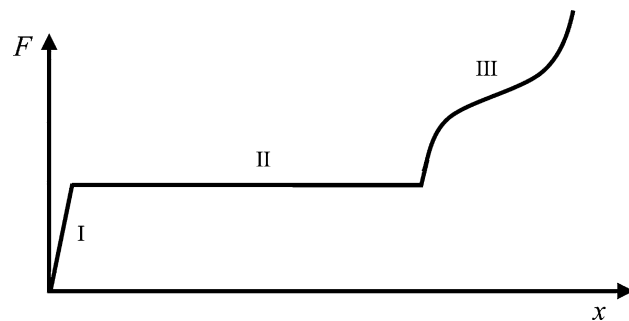


**Fig. 1** A schematic illustration of the elongation of a single P pilus with its three elongation regions

region III originates from an over-stretching of the linearized PapA rod, held together by a  $\beta$ -strand complementation between subsequent PapA units. Its particular form originates from a combination of an elastic elongation<sup>2</sup> of a linear biomolecular chain and a transition between two discrete conformations of the head-to-tail bond,<sup>3</sup> both strongly affected by entropic effects.

Andersson et al. (2006c) developed an analytical model, based upon the sticky-chain concept, that describes the elongation of a pilus under strain/stress. The model is built upon a three-state energy landscape and treated the elongation by two sets of rate equations; one valid for regions I and II and the other for regions II and III. Each set of rate equations was solved analytically under steady-state conditions. The predicted force–elongation dependence for unfolding showed an excellent agreement with experimental data taken under steady-state conditions. The dynamic behavior was studied in a subsequent publication (Andersson et al. 2006a) and the model showed good agreement also with such data.

However, even though the sticky-chain model showed good agreement with measurements, it did not accurately describe the refolding “dip” that takes place in the phase transition from region III to II. This “dip” is assumed to originate from a lack of a nucleation kernel (a first layer in the helical structure) for folding to a quaternary structure (Fällman et al. 2005). In addition, the combined pilus-and-optical-tweezers system has an intricate self-regulating mechanical elongation behavior<sup>4</sup> that complicates

<sup>2</sup> Elastic elongation is here defined as the elongation that takes place under increased force when all bonds are in a given state. Elastic elongation can be, but is not necessarily restricted to be, linear with force.

<sup>3</sup> In the following referred to as opening and closure of the head-to-tail bond.

<sup>4</sup> In short, a stretching of a pilus gives rise to a force (or stress) in the system that tilts the energy landscape by lowering the barriers for bond opening. As the transition states are lowered the probability for bond opening increases, which increases the unfolding rate and decreases the refolding rate. This reduces the stress in the system, which, in turn, reduces the lowering of the transition state.

<sup>1</sup> Steady-state conditions are defined as those when the number of open and closed bonds follow an elongation or retraction adiabatically. Under these conditions, the force response becomes independent of the elongation speed.

analytical descriptions when dynamic processes are studied, if additional interactions between the individual units need to be included, or if also the behavior of the adhesion tip is to be considered.

As an alternative means to describe the unfolding and refolding mechanics of pili, applicable to both steady-state and dynamic conditions, we present in this work Monte Carlo (MC) simulations of the elongation and retraction (including unfolding and refolding) of P pili exposed to strain. Such simulations have previously been used to reproduce the unfolding of type 1 pili (Miller et al. 2006). However, those simulations were based upon a two-state serial model, which implies that they are unable to correctly predict the constant force–elongation behavior of region II or the wave-like shape of region III of P pili. In contrast, our model is based upon a three-state energy landscape with parallel bonds and does not have these limitations. The simulations are based upon the Metropolis algorithm, which compares the probability for a bond to open or close with a randomly generated number. The model parameters are adjusted so the simulations reproduce previously measured data for P pili. It is found that the MC simulations provide a convenient means to describe the force–elongation behavior for P pili under strain that does neither require an analytical solution, nor a numerical simulation, of the system of equations describing the interactions in the rod. They are therefore particularly suitable to such a self-regulating system as pili un- and re-folding. This opens up for the possibility to include also additional types of interactions in the rod, or to include the effect of other parts of the pili, e.g. the tip. The model could presumably also be used to simulate the behavior of other types of pili, e.g. type 1, since they have shown to have an architecture as well as force–elongation response that are similar to those of P pili (Andersson et al. 2007; Forero et al. 2006; Miller et al. 2006).

## Theory

### Polymer model

As was alluded to above, each pilus consists of a large number ( $\sim 10^3$ ) of PapA monomers,  $N_{\text{tot}}$ . Each unit is assumed to bind to its neighbors by one or two bonds that together can reside in either of three combined states, referred to as A, B, and C, with successively increased subunit distance as well as energy, as is schematically shown in the energy landscape diagram in Fig. 2. State A represents a closed layer-to-layer bond, which automatically implies that also the head-to-tail bond is closed. State B represents an open layer-to-layer bond, still with the head-to-tail bond in a closed conformation. State C, finally, represents the case when also the head-to-tail bond is open.

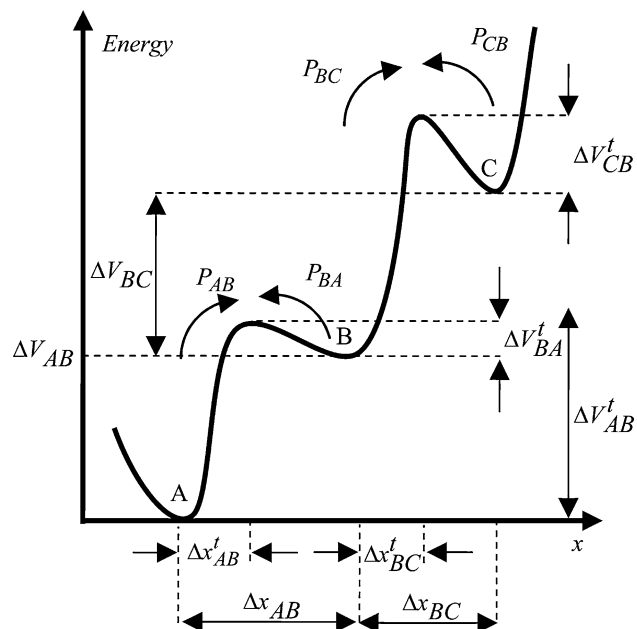


**Fig. 2** A schematic energy landscape diagram of a PapA unit and its bonds along the long axis of the pilus, also referred to as the reaction coordinate. The three-states, A, B, and C, represent a closed layer-to-layer bond, an open layer-to-layer bond together with a closed head-to-tail bond, and an open head-to-tail bond, respectively. The reaction coordinate, denoted by  $x$ , represents the projected distance between two PapA units along the long axis of the pilus

In the absence of strain, the pilus will be in its folded configuration, as is illustrated in panel A in Fig. 3, with all bonds in their lowest state, A. As the pilus is elongated, the stress in the system will increase, whereby the layer-to-layer bonds between consecutive layers in the helical structure will elongate elastically. This gives rise to the elastic behavior referred to as elongation region I, shown in Fig. 1.

When the stress in the system reaches a certain level, the helical structure starts to rupture. It has previously been shown that this takes place for forces around 27 pN under steady-state conditions (Andersson et al. 2006a, c; Fällman et al. 2005). However, as has been discussed previously (Andersson et al. 2006c), the mode of rupture is strongly governed by the quaternary structure of the pilus. The reason is that the helical structure of the PapA rod is mediated by several (3.28) layer-to-layer bonds per turn, whereas the outermost unit in the helical structure is attached to the rod through only one bond. An external force applied to the pilus is therefore distributed among several bonds in the interior of the rod, whereas the outermost bond experiences more or less the entire force. In addition, the opening of a layer in the interior of the pilus requires the simultaneous opening of at least three layer-to-layer bonds, which is highly unlikely. Both these effects lead to that the rupture of the layer-to-layer bonds in region II primarily takes place in a sequential manner at a force

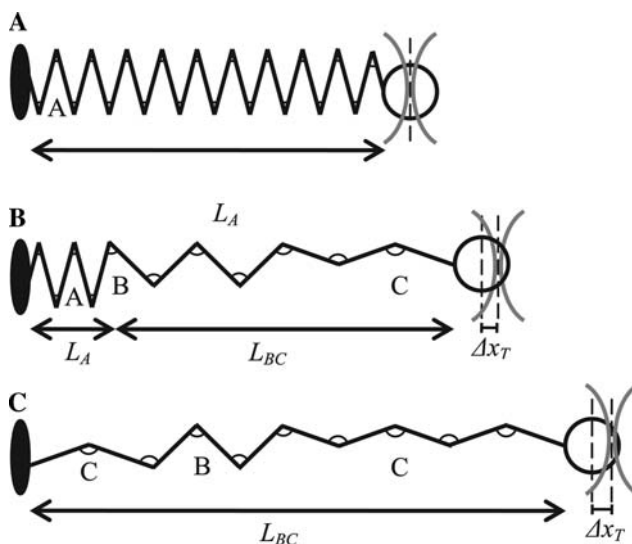


**Fig. 3** A two-dimensional illustration of a single pilus with subunits in state A, B, and C attached to a bead held in an optical trap. **a** The equilibrium position of the bead when no force is applied with the pilus in its native state. The pilus is here in region I and consists of a helixlike structure, whose length is  $L_A$ ; **b** a possible configuration of the units for a pilus in region II, in which an external force has partly linearized the pilus. The length of the linearized part of the pilus is  $L_{BC}$ . In **c** the pilus is fully linearized and is, therefore, in region III. The force response of the elongated pilus shifts the bead in the trap from its equilibrium position a distance  $\Delta x_T$

referred to as the unfolding force,  $F_{uf}$ , where the outermost closed head-to-tail bond is next to open and makes a transition from state A to B. This is schematically illustrated in panel B in Fig. 3. Region II, therefore, originates from pili in which one part is in its helical form, held together by closed layer-to-layer bonds (state A), whereas the other part is in a linearized form, built up of a number of (mostly closed) head-to-tail bonds (state B).

Under steady-state conditions, further elongation forces virtual all layer-to-layer bonds to open at the unfolding force before the head-to-tail bonds start to open. Region III, therefore, constitute a fully linearized pili, elongated to various degrees. However, since there are no parallel bonds in the linearized part of the pilus, the opening and closure of the head-to-tail bonds takes place in a random manner, which introduces entropic effects. It has become commonplace to describe the elongation of semi-flexible polymers exposed to stress by the worm-like chain (WLC) model (Bustamante et al. 1994; Marko and Siggia 1995). The elastic force–elongation response of the linearized part of the pilus is therefore described by such a model in this work.

#### Elongation model

As is described in more detail below, a typical force measurement is performed by increasing the distance

between the bacterium and the centum of the trap,  $x_{BT}$ , in small steps with a constant velocity. The bacterium-to-trap length is considered to be given by the sum of three parts;  $L_A$ , the total length of all units in state A,  $L_{BC}$ , the total length of the units in state B or C, and  $\Delta x_T$ , the displacement of the bead in the trap, i.e. as

$$x_{BT} = L_A + L_{BC} + \Delta x_T. \quad (1)$$

The sum of  $L_A$  and  $L_{BC}$  constitutes the instantaneous length of the pilus,  $L_{pili}$ . All lengths refer to the length projected onto the elongation axis.

Whereas all three lengths on the right hand side of Eq. (1) depend on the stress in the system,  $L_A$  and  $L_{BC}$  also depend on the number of bonds in each state. As the pilus is elongated, the stress in the system increases, which gives rise to alterations of  $L_A$  and  $L_{BC}$  by two effects, an elastic elongation and an opening and closure of bonds. Since the three lengths have their own unique elastic dependence of force as well as number of units in each state, they will be considered one by one.

For a given number of units in state A,  $L_A$  is given by the elastic force response of the part of the pilus in which the PapA units are in state A. The force from this part of the pilus,  $F_A$ , can be written as

$$F_A = k_A \left( \frac{L_A}{N_A} - l_A^0 \right), \quad (2)$$

where  $N_A$  is the number of units in state A,  $l_A^0$  the length of an individual unit in the absence of a force, and  $k_A$  an elastic constant for the elongation of a PapA unit in the rod. The initial value of  $L_A$  is  $N_A l_A^0$ . The force predicted by Eq. (2), with all bonds in their lowest state, i.e. with  $N_A$  equal to  $N_{tot}$ , corresponds to the linear response in region I in Fig. 1.

The length of  $L_{BC}$  is given by the units that are connected by bonds in either state B or C. As was alluded to above, this part of the pilus behaves like a semi-flexible polymer chain whose elasticity is described by the WLC model. This model predicts that there will be an entropic force,  $F_{BC}$ , opposing an elongation of the chain given by,

$$F_{BC}(L_{BC}) = \frac{kT}{l_p} \left[ \frac{1}{4} \left( 1 - \frac{L_{BC}}{L_{cl}} \right)^{-2} - \frac{1}{4} + \frac{L_{BC}}{L_{cl}} \right], \quad (3)$$

where  $l_p$  is the persistence length and  $L_{cl}$  the contour length of the chain of units that are either in state B and C. In our case the latter is given by

$$L_{cl} = N_B l_B + N_C l_C, \quad (4)$$

where  $N_B$  and  $N_C$  are the number of units in the states B and C, respectively, whereas  $l_B$  and  $l_C$  are the projected lengths for the units in the two states.  $L_{BC}$  is only implicitly given by the equation above.

Finally, the displacement of the bead in the trap,  $\Delta x_T$ , is given by

$$F_T = \kappa \Delta x_T, \quad (5)$$

where  $F_T$  is the force to which the bead is exposed and  $\kappa$  the elasticity constant of the trap.

It is assumed that viscous forces as well as inertial effects can be neglected. This implies that all forces in the system are in balance, i.e.  $F_A = F_{BC} = F_T = F$ . Combining the expressions above provides expressions for  $L_A$  and  $L_{BC}$ , and thereby  $L_{\text{pili}}$ , expressed solely in the bacterium-to-trap length,  $x_{BT}$ , and the number of bonds in the three states, i.e.  $N_A$ ,  $N_B$  and  $N_C$ .

For example, for a given bacterium-to-trap length,  $x_{BT}$ , and for a given number of bonds in the various states, i.e.  $N_A$ ,  $N_B$  and  $N_C$ ,  $L_{BC}$  is given by the solution to the expression

$$\frac{kT}{l_p} \left[ \frac{1}{4} \left( 1 - \frac{L_{BC}}{L_{\text{cl}}} \right)^{-2} - \frac{1}{4} + \frac{L_{BC}}{L_{\text{cl}}} \right] = \frac{\kappa (x_{BT} - L_{BC} - N_A l_A^0)}{1 + \kappa N_A / k_A}. \quad (6)$$

Inserting the value for  $L_{BC}$  into Eq. (3) provides an expression for the instantaneous force in the system,  $F$ , which in turn can be used in Eq. (2) to obtain a value of  $L_A$ . This provides, in turn, a value also for the length of the pili,  $L_{\text{pili}}$ .

#### Bond opening and closure model

As the pilus is elongated or retracted bonds will also successively open and close, effectively from state A via state B, eventually to state C, altering the response described above. The probability for bond opening is assumed to be proportional to the product of a thermodynamic attempt rate,  $v$ , and a Boltzmann factor expressed in terms of the height of an energy barrier,  $\Delta V_{ij}^t$  (Bell 1978). In the absence of an external force, a bond will make a transition from state  $i$  to state  $j$  with a thermal rate given by

$$k_{ij}^{\text{th}} = v e^{-\Delta V_{ij}^t / kT}, \quad (7)$$

where  $k$  is the Boltzmann factor and  $T$  the temperature.

When a bond is exposed to a force in the direction of the reaction coordinate the energy landscape is tilted. This implies that the transition barrier for bond opening decreases and the bond opening rate increases. In a similar way the bond closure rate decreases. The probability of a bond exposed to an external force,  $F$ , to make a transition under a short time interval,  $\Delta\tau$ , can then be expressed as

$$P_{ij}(F) = v e^{-(\Delta V_{ij}^t - F \Delta x_{ij}^t) / kT} \Delta\tau, \quad (8)$$

where  $\Delta x_{ij}^t$  is the distance from state  $i$  to the barrier, considered positive for bond opening and negative for bond closure (Bell 1978).

#### Simulation procedures

The simulation procedure was a slightly modified first-order Markov Chain Monte Carlo (MCMC) Metropolis algorithm. In the conventional MCMC Metropolis algorithm, the transition probability to change the system from state  $S_i$  to  $S_j$  is given by the ratio of the probabilities to be in the two states. In a thermodynamically driven system, the probability distribution is in general proportional to a Boltzmann factor of the type  $\exp(-V/kT)$ . The transition probability of a proposed change of the current state,  $S_i$ , to a new state,  $S_j$ , is therefore  $P_{ij} = \exp(-\Delta V_{ij}^t / kT)$ . The decision of accepting a transition is then based upon a comparison of this probability and a random number from a uniform distribution in the interval [0,1]. In the model used in this work, based upon the energy landscape picture, the probability for a transition is proportional to the energy difference between the current state and the transition state (which thus acts as a barrier), and not the final state. In addition to the Boltzmann factor for the transition state, the probability to make a change depends on the attempt rate and the time step, according to Eq. (8). Recognizing these differences, our method resembles the ordinary Metropolis algorithm.

The simulations were performed by moving the optical trap,  $x_{BT}$ , with a constant velocity, in small time steps. For each time step, the corresponding lengths of the two parts of the pilus,  $L_A$  and  $L_{BC}$ , as well as the force  $F$ , were calculated by the use of Eqs. (6), (3), and (2).<sup>5</sup> The new force alters the energy landscape and thereby the probability for bond transitions according to Eq. (8). Each unit is then given the possibility to change state according to the principle above. New values of the state numbers,  $N_A$ ,  $N_B$ ,  $N_C$  are calculated. The relevant parameter values are then saved and a new simulation step is performed. The time steps were chosen sufficiently small to make large changes to the system within each time step improbable.

As can be concluded from the description above, eight model parameters are needed to fully describe the energy landscape; four energy levels,  $\Delta V_{AB}^t$ ,  $\Delta V_{AB}$ ,  $\Delta V_{BC}^t$ , and  $\Delta V_{BC}$ , and four distances,  $\Delta x_{AB}^t$ ,  $\Delta x_{AB}$ ,  $\Delta x_{BC}^t$ , and  $\Delta x_{BC}$ . Other model parameters are the attempt rate,  $v$ , the temperature,  $T$ , the elasticity of the units in state A,  $k_A$ , the persistence length,  $l_p$ , the elongation velocity,  $\partial \Delta x_{BT} / \partial t$ ,

<sup>5</sup> In order to decrease the simulation time, simulations of elongation region I were performed directly from Eq. (2), thus with no reference to Eq. (3) or (6).

and the spring constant of the force transducer,  $\kappa$ , of which the latter two define the loading rate. In addition, each pilus has its specific number of subunits,  $N_{\text{tot}}$ .

## Results

The main aim of this work is to demonstrate the applicability of Monte Carlo simulations to describe the basic features of force–elongation of biomolecules exposed to strain, exemplified by P pili. A second aim is to assess values of the various model parameters that describe the elongation of P pili under strain. Since each parameter in the model has its own specific effect on the simulation, the values of the model parameters can be assessed by fitting the simulations to experimental data. Moreover, since the energies of the states are given by simulations under equilibrium, whereas the energies of the transition states are given by simulations of dynamical behavior, simulations of both equilibrium as well as non-equilibrium conditions need to be performed. The length parameters and  $N_{\text{tot}}$  originate from a fitting to the shape of region III and the length of region II of measurements performed under steady-state conditions, as well as from a fitting of the slope of a so called force–elongation speed plot measured with dynamic force spectroscopy (DFS). The elasticity of the PapA units in state A, finally, is given by the slope of region I. A number of simulations were performed, investigating elastic elongation as well as unfolding and refolding processes, under steady-state as well as dynamic conditions. The model parameters were furthermore individually optimized for every experimental curve in order to create a statistical basis for assessment of the mean values as well as the spread of the various parameter values.

### Unfolding steady-state conditions

The force response of single P pili under strain (i.e. for a forced elongations) have previously been investigated utilizing either optical tweezers or atomic force microscopy (Andersson et al. 2006a, b, c; Jass et al. 2004; Miller et al. 2006). The grey curve in Fig. 4 shows an example of a force–elongation curve of an individual pilus (referring to the elongation of the pilus length,  $L_{\text{pili}}$ ) stretched at constant speed (0.05  $\mu\text{m/s}$ ) by optical tweezers, performed with instrumentation previously described in the literature (Andersson et al. 2006a, b, c). The black curve displays a MC simulated force response for the set of parameters that gives rise to the best agreement with the experimental data. Since the elongation speed is below that at which dynamic effects set in (see discussion below), both curves represent

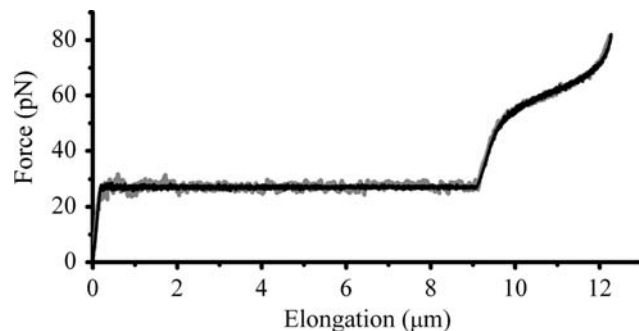


**Fig. 4** Force–elongation curves for an individual P pilus exposed to strain at an elongation speed of 0.05  $\mu\text{m/s}$ , which, for this system, represents steady-state conditions. The grey curve represents optical tweezers experiment, whereas the black line represents a Monte Carlo simulation

steady-state conditions. As can be seen in the figure, the simulations can well reproduce, in all three regions, experimental force–elongation curves of P pili measured under steady-state conditions.

As was alluded to above, the flat response of region II originates from a sequential opening (and sometimes also sequential closure) of the outermost closed (or opened) layer-to-layer bond. The unfolding forces of the layer-to-layer bonds of a simulation are presented as a histogram in Fig. 5. The solid line represents a fitted Gaussian distribution function. As can be seen from the figure, the distribution has the shape of a narrow Gaussian profile, in this case with a relative standard deviation of less than 1.5%. Such a small standard deviation verifies a previous hypothesis (Andersson et al. 2006a) that the unfolding process is a self-regulating opening and closure process that regulate the unfolding force to a value close to its mean.

The parameters  $\Delta V_{AB}$ ,  $\Delta V_{BC}$ ,  $\Delta x_{AB}$ ,  $\Delta x_{BC}$ ,  $k_A$ , and  $l_p$  describe the force–elongation behavior of P pili under steady-state conditions. The values of these parameters that minimized the discrepancy between the simulations and measurements, i.e. those that provided the best fit, are collected in Table 1. The values given represent averages over fits to eight steady-state curves. Values for the five first parameters have previously been assessed by the sticky-chain model (Andersson et al. 2006c). The values presented here are all, in general, within a few percent of those.<sup>6</sup> The value of  $l_p$ , which was adjusted so the slopes in the beginning and at the end of region 3 coincide with measured data, was not incorporated in the sticky-chain model. The good agreement with the previously assessed

<sup>6</sup> The value of  $\Delta V_{BC}$  given in Ref. Andersson (2006c) was specified to  $9 \pm 2 kT$ . However, this value represents the energy difference between state B and C in the presence of the unfolding force under steady-state conditions and it corresponds to a  $\Delta V_{BC}$  value, as defined in this work, in the absence of force, of  $15 \pm 3 kT$ .

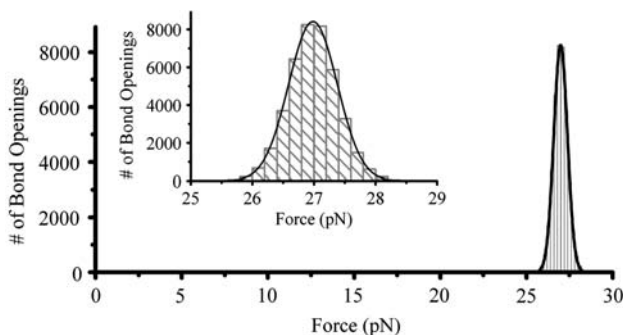


**Fig. 5** The force distribution of the unfolding of the quaternary structure under steady-state conditions from one simulation. The insert shows an enlargement of the part of the curve in which the data resides

**Table 1** Optimized model parameters values

Model parameter	Value
$\Delta V_{AB}$	$23.2 \pm 0.4 \text{ } kT$
$\Delta V_{BC}$	$14.5 \pm 0.4 \text{ } kT$
$\Delta x_{AB}$	$3.5 \pm 0.1 \text{ nm}$
$\Delta x_{BC}$	$0.90 \pm 0.02 \text{ nm}$
$k_A^a$	$660 \pm 200 \text{ pN/nm}$
$l_p$	$3.3 \pm 0.6 \text{ nm}$
$v$	$6 \times 10^9 \text{ Hz}$
$\Delta x'_{AB}$	$0.70 \text{ nm}$
$\Delta V'_{BC} / \Delta x'_{BC}$	$< 170 \text{ pN}$
$\Delta V'_{BA}$	$-1.5 \text{ } kT$

<sup>a</sup> This entity corresponds to  $3.28^2 k_A$  in (Andersson et al. 2006c). The value given here agrees to within 1 % with the value given in that work

parameter values verifies that the MC simulations of P pili not only correctly reproduce experimental data but also that the simulations constitute a reliable model of the force–elongation behavior of P pili under steady-state conditions.

#### Unfolding dynamic conditions

Figure 6 shows a set of curves simulated for four different elongation speeds, representing, from below, 0.1, 1, 10 and 100  $\mu\text{m/s}$ . The figure illustrates that the simulations predict, in this range of elongation speeds, a clear dynamic response of the unfolding of the quaternary structure in region II, but no such effect in region III. This behavior is in good qualitative agreement with both model predictions and experiments.

The dynamic behavior of the model can be qualitatively understood as follows: As the bacterium-to-trap distance is increased with a user-controlled fixed elongation speed,

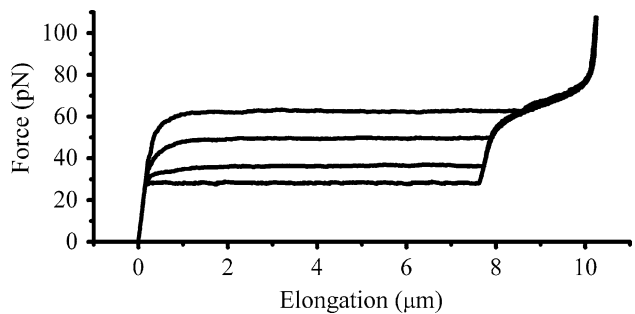


**Fig. 6** Simulated unfolding force–elongation response of a single pilus for four different elongation speeds, 0.1, 1, 10 and 100  $\mu\text{m/s}$ . The simulations predict unfolding forces in region II of 28, 36, 50 and 63 pN for these four speeds, respectively. The increase in the force in region II shows that the simulations predict a dynamic response of the elongation of P pili in this region. The fact that all four curves show an almost identical response in region III indicates that the simulations predict that there should be no dynamic response of P pili in region III for the range of velocities studied

given by  $\partial x_{BT} / \partial t$ , and under the condition that the force in the system does not change drastically, i.e.  $\partial \Delta x_T / \partial t \approx 0$ , the pilus will elongate at the same speed, i.e. with a  $\dot{L}_{pili}$  given by  $\partial x_{BT} / \partial t$ . Since each bond opening elongates the pili a given length, denoted by  $\Delta x_{AB}$  in region II and by  $\Delta x_{BC}$  in region III, the user-controlled elongating speed imposes an “effective” or “forced” bond opening rate in the pilus, given by  $\dot{L}_{pili} / \Delta x_{AB}$  and  $\dot{L}_{pili} / \Delta x_{BC}$  in the two regions, respectively.

The dynamic effect in region II originates from the fact that the forced bond opening rate of the outermost bond becomes significantly larger than the bond closing rate. Under these conditions, the force in the system will increase until the outermost bond experiences a bond opening rate, given by  $v \exp [-(\Delta V'_{AB} - F \Delta x'_{AB}) / kT]$ , that is equal to the forced bond opening rate,  $\dot{L}_{pili} / \Delta x_{AB}$ . As is shown in Andersson et al. (2006a), the dynamic effect sets in when the elongation speed,  $\dot{L}_{pili}$ , is larger than  $\dot{L}^* = \Delta x_{AB} k_{AB}^{\text{th}} \exp [(\Delta V_{AB} / kT) (\Delta x'_{AB} / \Delta x_{AB})]$ . Under these conditions, the force in the system is given by  $(kT / \Delta x'_{AB}) \ln (\dot{L}_{pili} / \Delta x_{AB} k_{AB}^{\text{th}})$ . This shows that there will be a clear dynamic response in region II, with an unfolding force that is proportional to the logarithm of the elongation speed.

The reason for the lack of dynamic effects in region III is that the pili in this region are composed of  $N_{\text{tot}}$  bonds in series (where  $N_{\text{tot}}$  is  $\gg 1$ , normally in the order of  $10^3$ ). Although the forced bond opening rate is virtually the same in this region, differing from that in region II only by any possible difference in bond length (i.e.  $\Delta x_{AB}$  vs.  $\Delta x_{BC}$ ), the pili will be elongated a distance  $\Delta x_{BC}$  by a bond opening as soon as any of the  $N_{\text{tot}}$  bonds open. Under the condition that  $\Delta V'_{BC}$  is not significantly larger than  $\Delta V'_{AB}$ , this takes place for a significantly lower force, namely the force for

which the opening rate of a given bond only is a fraction ( $1/N_{\text{tot}}$ ) of that in region II, on the average  $(\dot{L}_{\text{pili}}/\Delta x_{\text{BC}})/N_{\text{tot}}$ . This implies that the dynamic effects in region III will be roughly three orders of magnitude smaller than those in region II and that they are expected to set in at considerably higher elongation speeds than in region II. The simulated force–elongation response is thereby in good quantitative agreement with the prediction of the model.

The dynamic effects of P pili unfolding have been investigated experimentally by Andersson et al. (2006a). In short, it was found that there is a dynamic effect in the force–elongation behavior of P pili in region II but no such effect in region III, in good agreement with both the model predictions and the simulations given in Fig. 6. It was furthermore found that the unfolding force in region II shows a dynamic effect for elongation speeds roughly above 0.4  $\mu\text{m/s}$ . The simulations are therefore also in good qualitative agreement with the experimental findings performed in Andersson et al. (2006a).

In order to obtain quantitative information from the simulations under dynamic conditions, the unfolding force in region II was assessed for a large number of elongation velocities and the results were compared to previous DFS measurements (Andersson et al. 2006a). Figure 7 displays a set of measured force–elongation speed data points (filled circles) together with simulated data points (open triangles). The simulations indicate that the unfolding force increases from 28 pN to around 63 pN as the elongation speed is increased five orders of magnitude (from 0.001 to 100  $\mu\text{m/s}$ ). As can be seen from the figure, the simulations agree well with experimental data for the range of elongation speed in which data is available, i.e. from 0.1 to 100  $\mu\text{m/s}$ .

There is, unfortunately, no experimental data available for elongation speeds below 0.05  $\mu\text{m/s}$ , caused by the fact that the instrumentation did not allow movements at such

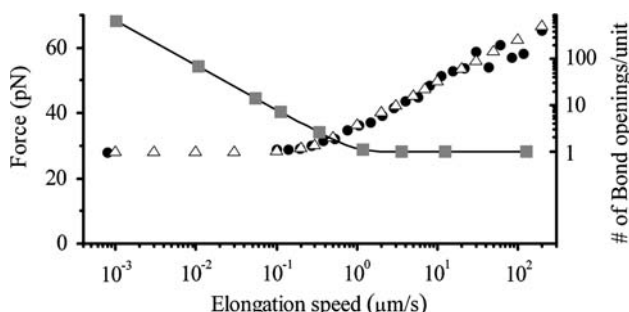


**Fig. 7** Unfolding force of the quaternary structure (region II) of P pili as a function of elongation speed for experimental data (filled circles) and simulations (open triangles), both left axis. The filled squares (right axis) show the average number of times a given layer-to-layer bond opens during an elongation event. The experimental data is taken from (Andersson et al. 2006a)

low speeds. The simulations for the lowest elongation speeds ( $<0.05 \mu\text{m/s}$ ) agree, however, with the force by which the pilus has to be stretched to be held at a fixed length, which is represented by the data point (the filled circle) that is inserted in the leftmost part of the figure. On the other hand, since the measurements at 0.1  $\mu\text{m/s}$  agree with those when the pilus was held at a fixed length, it is assumed that all unfolding forces in this region are the same. This implies that the simulations under dynamic conditions are in good quantitative agreement with experiments performed also in the lower range of elongation velocities.

As was alluded to above, fits of the simulations to data taken under dynamic conditions can provide information about the thermal bond opening rate and the position of the transition barrier between the states A and B. Also the parameters from the dynamic simulations are collected in Table 1. The values given originate from fits to 24 sets of data, measured under dynamic conditions. The simulations predict a length of the layer-to-layer bond,  $\Delta x_{\text{AB}}^t$ , of 0.70 nm, which is in good agreement with that evaluated by the sticky-chain model from the measurements in (Andersson et al. 2006a),  $0.76 \pm 0.11 \text{ nm}$ . The simulation predicts also a value of  $\Delta V_{\text{AB}}$  of  $23.2 \pm 0.4 \text{ kT}$  and a transition height,  $\Delta V_{\text{AB}}^t$ , of  $21.7 \pm 0.4 \text{ kT}$  for an attempt rate of  $6 \times 10^9 \text{ Hz}$ . The analysis in (Andersson et al. 2006a) assessed  $\Delta V_{\text{AB}}$  to  $23 \pm 1 \text{ kT}$ , whereas  $\Delta V_{\text{AB}}^t$  was considered to be within  $kT$  from this, all for an attempt rate of  $10^{10} \text{ Hz}$ . The dynamic response of the simulations are therefore also in reasonably good quantitative agreement with measurements evaluated by the sticky-chain model.

The simulations provide also a possibility to assess the average number of bond transitions (openings and closures) for each layer-to-layer bond in region II under a specific set of condition. The curve represented by filled squares in Fig. 7 shows that a layer-to-layer bond opens on the average a considerable number of times ( $>10$ ) for low elongation speeds ( $<0.1 \mu\text{m/s}$ ), whereas they open only once in the dynamic regime (i.e. for elongation speeds above  $\sim 1 \mu\text{m/s}$ ). This originates from the fact that the refolding balances the unfolding rate under steady-state conditions, whereas it plays an insignificant role under dynamic conditions. More specifically, the simulations show that for an elongation speed of 0.01  $\mu\text{m/s}$  every bond opens on the average  $\sim 70$  times for each net bond opening, which implies that the bond opening rate is around  $\sim 200 \text{ Hz}$  for elongation speeds below  $L^*$ .

In line with the model predictions from above, no dynamic response of region III has been found experimentally for P pili, despite the use of elongation velocities up to 100  $\mu\text{m/s}$  (corresponding to a loading rate of around 14 nN/s). Experiments have therefore not been able to assess any values of the energy of the transition state,

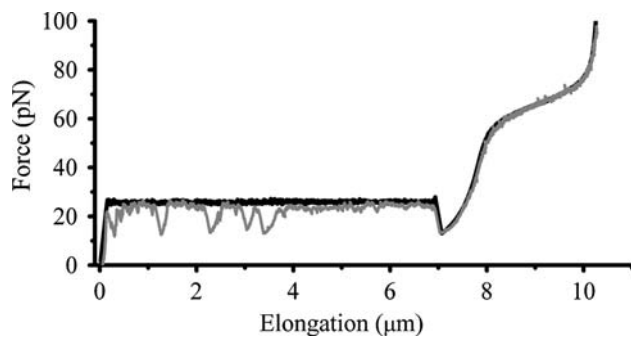


**Fig. 8** The refolding of a P pilus under steady-state conditions with an elongation speed of 0.05  $\mu\text{m/s}$  for optical tweezers experiment (grey curve) and Monte Carlo simulated data (black line)

$\Delta V_{\text{BC}}^t$ , or its position,  $\Delta x_{\text{BC}}^t$ . It is consequently not possible to assess any values of these parameters from the simulations. On the other hand, the simulations can provide an upper limit of the ratio between the two, i.e.  $\Delta V_{\text{BC}}^t/\Delta x_{\text{BC}}^t$ , of 170 pN.

#### Refolding

Simulations of refolding have also been performed. Under equilibrium conditions, the refolding curve retraces the unfolding curve with the exception of the dip between region III and II. Figure 8 shows a typical experimental refolding curve together with a simulation based upon the model parameters given in Table 1. The experimental data corresponds to the same pilus that was used in Fig. 4. As can be seen from the figure, the model is capable of predicting also the dip that appears when the pilus is contracted from region III to region II. This hysteresis is caused by the lack of a nucleation kernel for the refolding of the quaternary structure, which impedes the initiation of the refolding of the rod (Fällman et al. 2005). However, the MC model is not able to simulate, based upon fundamental interactions, the initiation of the refolding of the quaternary structure; in order to obtain the subsequent sequential refolding of the PapA rod, this instantaneous refolding was initiated by an artificial introduction of a nucleation kernel. The other spontaneously occurring dips in the retraction curve, which are assumed to originate from stochastic misfoldings, cannot be predicted by the MC simulation in its present form since no provision for any such spontaneous misfolding has been given in the model.

#### Discussion

The present work has shown that MC simulations based upon a three-state energy landscape in combination with

Bells theory for bond transitions can successfully describe the elongation and retraction behavior of P pilus exposed to strain. It has been demonstrated that the MC simulations agree well with experimental data for P pilus measured by optical tweezers under both steady-state and dynamic conditions. Both the initial elastic response as well as the zipper-like unfolding of the layer-to-layer bonds (region II) are well reproduced. Moreover, the model can also describe the wave-like shape of region III, which originates from a combination of entropic elongation and an opening of the head-to-tail bond, as well as the dip that appears during retraction from region III to II.

#### Steady-state elongation

MC simulations of pili elongation based upon a two-state model have previously been performed by Miller et al. (2006). However, that model fails in predicting the correct unfolding force in region II because the layer interactions were not modeled as several parallel bonds, which does not necessarily give rise to a sequential unfolding. The model therefore predicts a force that increases monotonically with the decreasing number of folded units. This is clearly in contrast to measurements, which indicate that the unfolding takes place under a constant force (Andersson et al. 2006c; Jass et al. 2004). In addition, a two-level model is unable to describe the wave-like force–elongation behavior seen in region III.

However, the three-state model with 3.28 parallel bonds per turn used in this work does not suffer from such shortcomings. It was shown above that the simulations predict that the self-regulating sequential unfolding in region II takes place under constant force (i.e. a flat response), with only minor fluctuations  $\sim 0.4$  pN around the mean value, which is fully in line with experimental findings (Andersson et al. 2006c). Besides, it is interesting to note that the force–elongation behavior for pili in region II is vastly dissimilar from that given by the theory for single bonds, which predicts a large variation of the rupture force (Evans 1998).

The simulation was also fitted to region III. It has been found that the center part, consisting of an inclined plateau, is mainly given by the entropic contribution from the opening of the head-to-tail bond, i.e. the transition from states B to C (Andersson et al. 2006c). However, it has been suggested that the outermost parts of region III are significantly affected by the entropy originating from elastic elongation. The good agreement between the simulations and the measurements presented in this work supports all this, i.e. that region III originates from a combination of elastic/entropic stretching of a linear polymer (thus described by the WLC model) and a stochastic bond opening and closure of the head-to-tail bond.

Using the parameter values from Table 1, it can be estimated that the opening and closure rates for the layer-to-layer bonds are around  $\sim 200$  Hz when a pilus is stretched with the steady-state unfolding force, irrespectively of the elongation speed. It is also interesting to note that the persistence length for P pili assessed in this work, which is  $3.3 \pm 0.6$  nm, agrees well with that of type 1 pili estimated by Miller et al. (2006)  $3.3 \pm 1.6$  nm. This indicates that the basic mechanical backbone structures of these two types of pili are rather similar. It could finally also be noted that the MC simulations predict that the bond opening length between the states B and C is around  $0.90 \pm 0.02$  nm, which is in agreement with the value that was assessed by the sticky-chain model by Andersson et al. (2006c),  $0.94 \pm 0.05$  nm.

### Dynamic elongation

As was shown above, for the set of parameter values presented in Table 1, the Monte Carlo simulations of the dynamic response of the unfolding of the quaternary structure agree well also with DFS measurements previously performed by Andersson et al. (2006a). To best reproduce the DFS measurements displayed in Fig. 6, the energy barrier,  $\Delta V_{BA}^r$ , had to be set to a negative value, viz.  $-1.5 kT$ . This supports a previous hypothesis that state B is not a bound state in the absence of force, but that it emerges as a bound state as an applied force tilts the energy landscape (Andersson et al. 2006a). Moreover, under the assumption that the attempt rate is close to that for bonds in solutions,  $6 \times 10^9$  Hz (Evans 2001), it was found that the simulations predict a value of the energy of the layer-to-layer bond of  $23 kT$ . These two features indicate that the rod is held together by strong bonds. It also implies that the thermal bond opening rate in the absence of applied force,  $k_{AB}^{\text{th}}$ , takes a value of around 0.5 Hz, whereas the layer-to-layer bond closure rates reach the attempt rate in the absence of a barrier. The large difference in thermal rates supports the hypothesis that it is unlikely that the rod unfolds spontaneously, and that its function instead is solely for mechanical action, i.e. for taking up external forces, e.g. shear forces created by the urine flow.

Moreover, the simulations under dynamic conditions indicate that the distance to the energy barrier,  $x_{AB}^r$ , is 0.70 nm, which is in reasonable agreement with that assessed by DFS by Andersson et al. (2006c) using the sticky-chain model (0.76 nm). In view of the fact that the experimental data for the highest elongation speeds scatter significantly (see Fig. 7), a difference in barrier distance of 10% can be seen as acceptable. This illustrates not only that the well known fact that the unfolding force follows a logarithmic increase for higher elongation

speeds, as the model predicts, but also that simulations provide a good complement to the sticky-chain model for assessment of model parameters also under dynamic conditions.

### Refolding

It was moreover shown above that the three-state MC simulation procedure presented here also could reproduce the refolding of a pilus in an acceptable way. For elongation and retraction speeds below those for steady-state conditions, the retraction was found to retrace the elongation behavior completely, with one single but clear exception; a dip during retraction from regions III to II. It has been hypothesized that this dip originates from what used to be called “a lack of nucleation kernel for the onset of the folding of the quaternary structure” (Andersson et al. 2006b; Fällman et al. 2005). The present MC simulation model provides a convenient means to support this hypothesis.

The basis of this hypothesis is as follows: After a full linearization of the quaternary structure, i.e. when the pilus has been elongated into region III, all layer-to-layer bonds are open. This implies that there are no longer any  $n$ th and  $(n+3)$ th subunits that are in close proximity to each other; the  $n$ th subunit has only the  $(n-1)$ th and  $(n+1)$ th units as its closest neighbors through the head-to-tail bond. This reduces significantly the probability for closure of a bond between any  $n$ th and  $(n+3)$ th subunits, i.e. the formation of a layer-to-layer bond. Therefore, in order for the first layer-to-layer bond to close during retraction of a fully linearized pilus (panel C in Fig. 3), the force in the system has to be lowered to such a level that a thermal fluctuation can give rise to an occasional closure of a layer (implying that a pair of  $n$ th and  $(n+3)$ th subunits somewhere in the pilus have to get in sufficient proximity to each other). Since this takes place only for a force significantly lower than the normal unfolding force,  $F_{\text{uf}}$ , a dip in the force–elongation curve during retraction from region III to region II is expected. On the other hand, as soon as the first layer has been created, neighboring units will quickly refold in a zipper mode of refolding until the force reaches the unfolding force under steady-state conditions. This closure phenomenon is assumed to typically involve the refolding of  $\sim 10\%$  of the subunits. However, no attempt was made in this work to model this onset of refolding, since it was assumed that this would require a more sophisticated binding model than the one-dimensional three-state model that has been used in this work.

Although no mechanisms for the onset of the quaternary structure of the P pili were included in the MC

model in this work, the hypothesized sequence of events for the retraction dip of P pili could be verified by the MC simulations. As seen in Fig. 7, the simulated refolding curve follows the experimental data in region III closely. This indicates that the form of the dip is well described by the WLC model, which dominates the outermost part of region III, and supports the assumption that the form of the retraction dip is dominated by entropic elongations.

It seems unlikely that any unfolding of the PapA tertiary (backbone) structure can take place for the range of forces typically applied by optical tweezers or used in the simulations since it has been shown that the strong link (consisting of van der Waals and hydrophobic energy) between subunits can extend forces up to 500 pN (Forero et al. 2006; Miller et al. 2006). In addition, it has also been shown that FimA units (which corresponds to the PapA units in type 1 pili) resist both denaturants and boiling (Forero et al. 2006; Miller et al. 2006). Experiments that in part support this hypothesis have been done by Andersson et al. (2006b). The authors showed that long time strain measurements ( $>1$  h) of the PapA rod do not compromise the mechanical properties of P pili. The MC simulations have therefore not included any unfolding of the tertiary structure of the P pili.

Although several of the results presented above confirm, to a large degree, previous assessments of P pili obtained by the use of the sticky-chain model, the MC simulation methodology presented here have certain advantages over that model. One is that it can directly provide information about the steady-state as well as the dynamic behavior of such a complicated self-regulating system as the pilus-optical-tweezers system constitute. In addition, it can provide information about the stochastic noise in the system. The MC simulations can also possibly rather easily be expanded to include the function of the tip and/or the adhesin, which will give rise to an even better understanding of the intrinsic behavior of a single pilus. This implies that MC simulations can open up the possibility to model cooperative multi-pili bindings, which is assumed to be of highest importance for the biomechanical response of UPEC bacteria *in vivo*.

**Acknowledgments** The authors acknowledge Erik Fällman for fruitful discussions. This work was supported by the Swedish Research Council under the project 621-2005-4662 and made within the Umeå Center for Microbial Research (UCMR). Economical support for the construction of a force measuring optical tweezers system from the Kempe foundation and from Magnus Bergvall's foundation is acknowledged.

## References

Andersson M, Fällman E, Uhlin BE, Axner O (2006a) Dynamic force spectroscopy of the unfolding of P pili. *Biophys J* 91:2717–2725

Andersson M, Fällman E, Uhlin BE, Axner O (2006b) Force measuring optical tweezers system for long time measurements of Pili stability. *SPIE* 6088:286–295

Andersson M, Fällman E, Uhlin BE, Axner O (2006c) A sticky chain model of the elongation of *Escherichia coli* P pili under strain. *Biophys J* 90:1521–1534

Andersson M, Uhlin BE, Fällman E (2007) The biomechanical properties of bacterial pili that mediate *E. coli* adhesion to host tissue reflect their infection environment. *Biophys J.* 93. doi: [10.1529/biophysj.107.110643](https://doi.org/10.1529/biophysj.107.110643)

Bell MG (1978) Models for the specific adhesion of cells to cells. *Science* 200:618–627

Bullitt E, Makowski L (1995) Structural polymorphism of bacterial adhesion pili. *Nature* 373:164–167

Bullitt E, Makowski L (1998) Bacterial adhesion pili are heterologous assemblies of similar subunits. *Biophys J* 74:623–632

Bustamante C, Marko JF, Siggia ED, Smith S (1994) Entropic elasticity of lambda-phage DNA. *Science* 265:1599–1600

Evans E (1998) Energy landscapes of biomolecular adhesion and receptor anchoring at interfaces explored with dynamic force spectroscopy. *Faraday Discuss* 111:1–16

Evans E (2001) Probing the relation between force—lifetime—and chemistry in single molecular bonds. *Ann Rev Biophys Biomol Struct* 30:105–128

Fällman E, Schedin S, Jass J, Andersson M, Uhlin BE, Axner O (2004) Optical tweezers based force measurement system for quantitating binding interactions: system design and application for the study of bacterial adhesion. *Biosens Bioelectron* 19:1429–1437

Fällman E, Schedin S, Jass J, Uhlin BE, Axner O (2005) The unfolding of the P pili quaternary structure by stretching is reversible, not plastic. *EMBO Rep* 6:52–56

Forero M, Yakovenko O, Sokurenko EV, Thomas WE, Vogel V (2006) Uncoiling mechanics of *Escherichia coli* type I fimbriae are optimized for catch bonds. *PLoS Biol* 4:1509–1516

Gong MF, Makowski L (1992) Helical structure of P pili from *Escherichia coli*—evidence from X-ray fiber diffraction and scanning-transmission electron-microscopy. *J Mol Biol* 228:735–742

Jass J, Schedin S, Fällman E, Ohlsson J, Nilsson U, Uhlin BE, Axner O (2004) Physical properties of *Escherichia coli* P pili measured by optical tweezers. *Biophys J* 87:4271–4283

Johnson JR, Russo TA (2002) Uropathogenic *Escherichia coli* as agents of diverse non-urinary tract extraintestinal infections. *J Infect Dis* 186:859–864

Marko JF, Siggia ED (1995) Stretching DNA. *Macromolecules* 28:8759–8770

Miller E, Garcia TI, Hultgren S, Oberhauser A (2006) The mechanical properties of *E. coli* type 1 Pili measured by atomic force microscopy techniques. *Biophys J* 91:3848–3856

Soto GE, Hultgren SJ (1999) Bacterial adhesins: common themes and variations in architecture and assembly. *J Bacteriol* 181:1059–1071

Thomas WE, Trintchina E, Forero M, Vogel V, Sokurenko EV (2002) Bacterial adhesion to target cells enhanced by shear force. *Cell* 109:913–923